Creeplike behavior in athermal threshold dynamics: Effects of disorder and stress

Subhadeep Roy* and Takahiro Hatano†
Earthquake Research Institute, University of Tokyo, 1-1-1 Yayoi, Bunkyo, 113-0032 Tokyo, Japan

(Received 31 October 2017; revised manuscript received 4 June 2018; published 27 June 2018)

We study the dynamical aspects of a statistical-mechanical model for fracture of heterogeneous media: the fiber bundle model with various interaction ranges. Although the model does not include any nontrivial elementary processes such as nonlinear rheology or stochasticity, the system exhibits creeplike behaviors under a constant load being slightly above the critical value. These creeplike behaviors comprise three stages: primary, secondary, and tertiary. In the primary and tertiary stages, the strain rate exhibits power-law behaviors with time, which are well described by the Omori-Utsu and the inverse Omori laws, respectively, although the exponents are larger than those typically observed in experiments. A characteristic time that defines the onset of power-law behavior in the Omori-Utsu law is found to decrease with the strength of disorder in the system. The analytical solution, which agrees with the above numerical results, is obtained for the mean-field limit. Beyond the mean-field limit, the exponent for the Omori-Utsu law tends to be even larger but decreases with the disorder in the system. Increasing the spatial range of interactions, this exponent is found to be independent of disorder and to converge to the mean-field value. In contrast, the inverse Omori law remains independent of the spatial range of interaction and the disorder strength.

DOI: 10.1103/PhysRevE.97.062149

I. INTRODUCTION

Creep is a slow plastic deformation process of materials realized at stress levels below the yield strength. In general, three distinct stages are known for the time evolution of the strain rate under constant stress. After the stress is applied to a specimen at $t = 0$, the strain rate decreases with time, obeying a power law, t^{-p} [1]. This stage is referred to as primary creep and it is followed by secondary creep with nearly time-independent strain rate. In subsequent tertiary creep, the strain rate increases as $(t_f - t)^{-p'}$, where t_f denotes the time of breakdown. The two exponents, p and p', are not generally the same, but typically range from 0.6 to 1.0 [2–5].

On the other hand, numerous microfracture events are detected as acoustic emissions (AE) particularly in primary and tertiary creep. The rate of AE events also obeys power laws that are similar to those for strain rate [3,6,7].

Interestingly, a power law similar to that of primary creep is known for the statistics of earthquakes: the Omori-Utsu law [8,9]. This describes the rate of aftershocks decreasing in a power-law fashion with the time elapsed from a main shock: $n(t) \propto (t + c)^{-\alpha}$, where $n(t)$ is the aftershock rate as a function of the elapsed time t from a main shock and c is the time constant. The exponent α varies from 0.7 to 1.6 [9,10], while the c value may depend on the main shock magnitude and a magnitude cutoff for aftershocks [11].

Following this nomenclature, the power laws describing the acceleration of AE event rate in the tertiary creep stage has been referred to as the inverse Omori law. Avoiding the singulariry at the time of breakdown ($t = t_f$), the inverse Omori law may be written as $n(t) \propto (t_f - t + c')^{-\alpha'}$, where $n(t)$ is the rate of AE events, t_f is the time of breakdown, and c' is the time constant. Note that the inverse Omori law is not usually observed for earthquakes [12], whereas it is common in material failure.

Although the Omori-Utsu and the inverse Omori laws originally describe the rate of AE events, their functional forms are also applicable to the behaviors of strain rate. In this study, we thus refer to these laws in terms of the strain rate. Namely, the Omori-Utsu law for primary creep and the inverse Omori law for tertiary creep read, respectively,

$$\dot{\epsilon}(t) \propto (t + c)^{-p}, \tag{1}$$

$$\dot{\epsilon}(t) \propto (t_f - t + c')^{-p'}. \tag{2}$$

Here we use four exponents: p and p' for the strain rate, and α and α' for the AE (or seismic) event rate, respectively. No general correlations have been found between these four exponents [3]. Here we focus on the behavior of strain rate and therefore p and p' are our concern.

To our knowledge, the time constant c in Eq. (1) has not been estimated quantitatively for creep tests. In the context of earthquakes, it is referred to as the c value exhibiting the systematic dependence on the stress state of the system [13,14]. Therefore, estimate of the time constant c is also our interest here.

There have been some physical models that are addressed to reproduce the three stages of creep. Most of them are classified into the fiber bundle model [15–18]. This is an assembly of fibers that support the mechanical load in parallel. Each fiber has its own failure threshold, which is randomly set according to a specific probability distribution function. To describe the creep behaviors, some additional physical processes have been adopted. For instance, stochastic criteria have been used for

*sroy@eri.u-tokyo.ac.jp
†hatano@eri.u-tokyo.ac.jp

the elementary failure process, which may resemble thermal activation processes [19–23]. Another class of attempts is to assume rather macroscopic constitutive laws for each fiber: nonlinear vicoelastic rheology [2,3] or a damage accumulation process [24].

In the present study, we show that such additional physical processes are not necessary to reproduce three stages of creep (at least) semiquantitatively. The key idea is to introduce the time evolution in a simple fiber bundle model. The prototype is already known in the literature as a recursive dynamics [25]. It has been shown by Pradhan and Hemmer that the standard fiber bundle model with a recursive dynamics exhibits some interesting behaviors that look similar to creep [26]. However, they did not discuss the power-law behaviors and their analysis is limited to the mean-field limit.

Here we investigate the time evolution toward breakdown in a simple fiber bundle model under a constant load for both the mean-field and the local stress concentration cases. Although the model does not include any thermal activation process, it resembles most properties observed in creep tests including the above-mentioned three stages. Particularly, the Omori-Utsu and the inverse Omori laws are reproduced and the exponent p and the c value are obtained. We show the dependence of c value on the external load and disorder in the system.

In the next section, we provide a brief discussion of the model followed by the analytical results given in Sec. III. The numerical results for the mean-field limit as well as the local load-sharing model are discussed in details in Sec. IV. In the final section, we have discussed our findings in a broader context and summarized the chances of future works.

II. DESCRIPTION OF THE MODEL

Here we adopt a fiber bundle model, as in the previous studies. Initially, the L intact fibers support the load F in parallel, resulting in the stress of $f = F/L$ on each single fiber. Each fiber has its own fracture strength chosen randomly from a certain distribution. The dispersion of the fracture strength characterizes the disorder in the model. If the applied stress exceeds any of the threshold values, the corresponding fibers break irreversibly. After a rupture event, the load that has been supported by the broken fibers is redistributed among the remaining intact fibers. In this literature, two kinds of redistribution models are commonly used: (i) the global load-sharing (GLS) model, in which the load is redistributed equally among all the other surviving fibers [15,16], and (ii) the local load-sharing (LLS) model, in which the load is redistributed only to the surviving neighbors [27–32]. The GLS model is regarded as the mean-field model as the range of load redistribution is infinite.

In both the models, the stress on the unbroken fibers increases upon redistribution of the load and therefore a single rupture event can cause a cascade of further rupture events. At a given load of F, the system eventually comes to a stable state after a cascade of ruptures; otherwise all the fibers fail. In the former case, the load is increased slightly for a system to reach another stable state with less surviving fibers at larger stress. Such an increment process may be repeated until all the fibers break after a series of cascades. The repetition of the force increments enables one to define the critical load F_c, at which all the fibers are broken; namely, there are no stable states above the critical stress F_c. The value of F_c depends on the disorder in the system [33], described by dispersion in the strength of fibers. Note that it also depends on the system size L in the local load-sharing limit [20,34,35]. This conventional algorithm may correspond to a quasistatic process, as the system is always at the stable fixed point and evolves only when the load F is increased.

In this study, we investigate the time evolution of the model at a constant load, which is slightly above the critical value. The system is eventually led to breakdown under such a large load but we can still investigate the dynamics toward breakdown by introducing the relaxation time of the load redistribution. Namely, the breaking of fibers and the following load redistribution takes a certain lapse of time denoted by τ. This is regarded as a single time step here. Note that this time constant is assumed to be zero in a conventional algorithm [16]. In general, τ is interpreted as a relaxation time for the internal stress state of the system, and may depend on many physical ingredients such as the stress level, time or the temperature. Thus, the relaxation time τ may not be constant throughout the entire time evolution of the system partly because the number of intact fibers are decreasing gradually. Nevertheless, we regard τ as a constant throughout this work for simplicity, allowing analytical solutions for mean-field cases.

We adopt the following algorithm: the total load remains at $F(\approx F_c)$ throughout the time evolution. The initial stress is thus F/L at $t = 0$. Then the fibers having the strength lower than F/L should break and as a result the load is redistributed to all the remaining fibers (the GLS model) or only to the neighbors of the broken fibers (the LLS model). In any case, due to the load redistribution, some fibers are overloaded beyond their strength, resulting in further ruptures at the next time step, $t = \tau$. This defines a single time step in our algorithm and is repeated until all the fibers are broken.

The notion of avalanche is a bit different for our present work than the conventional model. We have defined an avalanche as number of fibers broken in between two consecutive redistributions. After the critical stress is applied, the model shows a big avalanche, leading to a sudden increase in strain. This can be considered to be equivalent to the main shock during a seismic event. After such big avalanche, the model evolves and gradually breaks with increasing time, producing a number of aftershock-like small avalanches. With such a definition of avalanches, the model is essentially the same as that investigated by Pradhan and Hemmer [26]. They investigated only the GLS but the dynamics of the system depends largely on the nature of load redistribution. In this paper, we investigate the time evolution in both models, the GLS and the LLS.

III. ANALYSIS ON GLOBAL LOAD-SHARING MODEL

In this section, the dynamics of the above mentioned GLS model, which is the mean field limit, is studied analytically. Note that the stress is identical for all the fibers in the GLS model. This allows one to discuss the system behavior analytically for some simple threshold distributions.

Writing the threshold distribution as $p(y)$, a general expression for the number of remaining fibers after the ith

$(i = 1,2,\dots)$ redistribution is

$$L_i = L_0 - \int_0^{f_{i-1}} L_0 p(y)dy. \tag{3}$$

where L_0 is the initial number of fibers, L_i is the number survived after the ith redistribution, and f_{i-1} is the force per fiber at the previous time step $i-1$. This can be rewritten in terms of fraction $n_i = L_i/L_0$

$$n_i = 1 - \int_0^{f_{i-1}} p(y)dy. \tag{4}$$

Using $n_i = f_0/f_i$, where f_0 is the strain at $t = 0$, the above equation is rewritten in terms of f:

$$f_i = \frac{f_0}{1 - \int_0^{f_{i-1}} p(y)dy} = \frac{f_0}{\int_{f_{i-1}}^{\infty} p(y)dy}. \tag{5}$$

This is the recursive relation for f. One can also consider a differential equation by using $(f_{i+1} - f_i)/\tau \simeq \dot{f}$, where τ is the duration of one time step, i to $i+1$:

$$\tau \dot{f} = \frac{f_0}{1 - \int_0^{f} p(y)dy} - f. \tag{6}$$

Therefore, the time evolution of the present system is solely determined by the threshold distribution $p(f)$ and the initial condition f_0. As $f_0 = F/L_0$, choosing f_0 is identical to determine the external load F. Note that f should be proportional to the strain of the system as the elastic modulus is supposed to be identical to all the fibers. Therefore, $\dot{f}$ should be proportional to the strain rate.

A. Uniform threshold distribution

For a uniform threshold distribution defined in $[f_{\max} - \delta, f_{\max}]$, the integral in Eq. (6) is easily solved to give

$$\tau \dot{f} = \frac{f_0 \delta}{f_{\max} - f} - f. \tag{7}$$

This is rewritten as

$$\tau \dot{f} = \frac{\left(f - \frac{f_{\max}}{2}\right)^2 + f_0\delta - \frac{f_{\max}^2}{4}}{f_{\max} - f}. \tag{8}$$

This is more simplified as

$$\tau \dot{x} = \frac{\left(x - \frac{1}{2}\right)^2 + \zeta}{1 - x}, \tag{9}$$

where

$$x := \frac{f}{f_{\max}}, \tag{10}$$

$$\zeta := \frac{f_0\delta}{f_{\max}^2} - \frac{1}{4}. \tag{11}$$

By choosing τ as the time unit, we realize that there is only one nondimensional parameter ζ that controls the time evolution of x.

(1) If ζ is nonpositive, Eq. (9) has steady-state solutions of $x = 1/2 \pm \sqrt{-\zeta}$: $x = 1/2 - \sqrt{-\zeta}$ is the stable fix point and the other is the unstable fix point. Starting from the initial condition $x_0 < 1/2 - \sqrt{-\zeta}$, the system relaxes to the stable fixed point exponentially. Although the time derivative of x is negative for x between these two fixed points, it should be interpreted as $\dot{f} = 0$ because the system is essentially irreversible.

(2) At $\zeta = 0$, the saddle-node bifurcation occurs. Namely, these two fixed points merge together and annihilate. This bifurcation is actually present for more general threshold distributions, and therefore they yield common behaviors near the bifurcation point.

(3) For positive ζ, there is no fixed point and the system undergoes breakdown. The exact solution of Eq. (9) is given as

$$t_m - t = \frac{1}{2}\log\left[\left(\frac{1}{2} - x\right)^2 + \zeta\right] + \frac{1}{2\sqrt{\zeta}}\tan^{-1}\left(\frac{1/2 - x}{\sqrt{\zeta}}\right), \tag{12}$$

where t_m is an integral constant. Here we consider a system close to the bifurcation point, $\zeta \ll 1$. Then the first term is negligible and one gets the following expression:

$$x \simeq \tfrac{1}{2} + \sqrt{\zeta}\tan[2\sqrt{\zeta}(t - t_m)]. \tag{13}$$

Because the above equation should give $x = x_0$ at $t = 0$,

$$t_m \simeq \frac{1}{2\sqrt{\zeta}}\tan^{-1}\left(\frac{1/2 - x_0}{\sqrt{\zeta}}\right). \tag{14}$$

The time evolution of the system is fully described by Eqs. (12) or (13). A practically important quantity is the time of breakdown, t_f, where the surviving fibers vanish: Namely, the force per fiber diverges. Considering Eq. (12), the time of the breakdown is given by

$$2\sqrt{\zeta}(t_f - t_m) = \pi/2. \tag{15}$$

Importantly, Eq. (12) implies both the Omori-Utsu and inverse Omori laws for the primary and the tertiary stages, respectively.

1. The Omori law

The primary stage is characterized by $x_0 < 1/2$. In this case $(1/2 - x_0)/\sqrt{\zeta} \gg 1$ and therefore $t_m \simeq \pi/4\sqrt{\zeta}$. We can thus write

$$2\sqrt{\zeta}t_m = \frac{\pi}{2} - f(x_0), \tag{16}$$

where $f(x_0) > 0$. By inserting Eq. (16) into Eq. (12),

$$x \simeq \frac{1}{2} - \frac{\sqrt{\zeta}}{\tan[2\sqrt{\zeta}t + f(x_0)]} \simeq \frac{1}{2} - \frac{1}{2t + f(x_0)/\sqrt{\zeta}} \tag{17}$$

for small t. Taking the initial condition into account, this leads to

$$x \simeq \frac{1}{2} - \frac{1}{2[t + 1/(1 - 2x_0)]}. \tag{18}$$

Therefore,

$$\dot{x} \simeq \frac{1}{2[t + 1/(1 - 2x_0)]^2}. \tag{19}$$

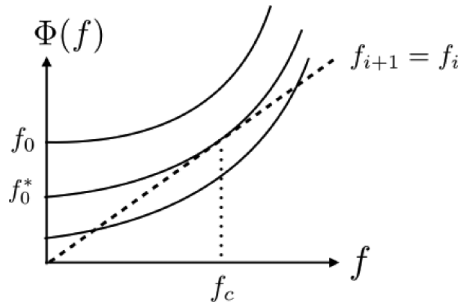

FIG. 1. Variation of the function $\Phi(f)$ with increasing force per fiber, f. The time evolution is given by $f_{i+1} = \Phi(f_i)$ and f_0 is the initial condition for f. Note that $\Phi(0) = f_0$. The plots are shown for $f_0 < f_0^*$, $f_0 = f_0^*$, and $f_0 > f_0^*$ (from the bottom to the top), respectively.

This is the Omori law with $p = 2$ and

$$c = \frac{1}{1 - 2x_0}. \tag{20}$$

We are thus led to the concrete expression for the c values.

2. The inverse Omori law

Inserting Eq. (15) into Eq. (12) and rewriting the time t as $t = t_f - t'$, one can get

$$x \simeq \frac{1}{2} + \sqrt{\zeta}\tan\left[\frac{\pi}{2} - 2\sqrt{\zeta}t'\right] \simeq \frac{1}{2} + \frac{1}{2(t_f - t)}. \tag{21}$$

This leads to the accelerating creep in the tertiary regime:

$$\dot{x} \simeq \frac{1}{2(t_f - t)^2}. \tag{22}$$

Note that the c value is not visible in this tertiary stage, whereas a nonzero c value is obtained in the primary stage.

B. General relation between saddle-node bifurcation and the power-law behaviors

We discuss more general threshold distributions taking advantage of saddle-node bifurcation. First, we discuss the nature of fixed points, which are the solutions of the following equation:

$$f = \Phi(f), \tag{23}$$

$$\Phi(f) = \frac{f_0}{\int_f^\infty p(y)dy}. \tag{24}$$

Since $p(y)$ is positive, $\Phi(f)$ is a monotonically increasing function of f. Because $\Phi(0) = f_0 > 0$, Eq. (23) may have some solutions. This is schematically shown in Fig. 1.

Let us suppose that saddle-node bifurcation occurs as a critical initial stress, $f_0 = f_0^*$. Then, because $\Phi(f)$ is tangent to f at the bifurcation point, one can consider an expansion of $\Phi(f)$ around $f = f_c$.

$$\Phi(f) \simeq f_c + (f - f_c) + a(f - f_c)^2 + \cdots, \tag{25}$$

where $a := \frac{1}{2}\partial^2\Phi/\partial f^2|_{f_c}$ is assumed to be positive. If f_0 is only slightly larger than f_0^*, one may write

$$\Phi(f) \simeq \zeta + f_c + (f - f_c) + a(f - f_c)^2 + \cdots, \tag{26}$$

where $\zeta > 0$. Truncating the above expansion at the second order, one can write an approximate time evolution equation:

$$\tau\dot{f} = \Phi(f) - f \simeq \zeta + a(f - f_c)^2. \tag{27}$$

This equation is integrated by separating the variables and gives

$$\sqrt{a\zeta}(t - t_1) = \arctan\left[\sqrt{\frac{a}{\zeta}}(f - f_c)\right] - \arctan\left[\sqrt{\frac{a}{\zeta}}(f_1 - f_c)\right], \tag{28}$$

where f and f_1 denote $f(t)$ and $f(t_1)$, respectively. Choosing $t_1 = t_m$ and $f(t_m) = f_c$, this equation reduces to

$$f(t) = f_c + \sqrt{\frac{\zeta}{a}}\tan[\sqrt{a\zeta}(t - t_m)], \tag{29}$$

which is identical to Eq. (12). Therefore, one can obtain the Omori-Utsu and the inverse Omori laws in the same manner as shown in the previous subsection. Particularly,

$$\dot{f} = \frac{\tau/a}{[t + \tau/a(f_c - f_0)]^2}. \tag{30}$$

Therefore, the exponent 2 should be robust for a wide class of systems that undergoes saddle-node bifurcation. The time constant c for the Omori law is given by

$$c = \frac{\tau}{a(f_c - f_0)}. \tag{31}$$

In the above discussion, the positiveness of a is crucial. Note also that these power-law behaviors are realized only in a finite range of f where the expansion of Eq. (25) can be truncated at the second order. Namely, Eq. (27) must hold in a sufficiently wide range of f for the realization of power-law behaviors. This implies that the saddle-node bifurcation itself is not a sufficient condition for the power-law behaviors. This valid range of the quadratic approximation and the sign of a depend on the detail of $p(f)$, and therefore we discuss this for some examples in the next subsection. Importantly, in some special cases the inverse Omori law can be observed without saddle-node bifurcation. Therefore, the bifurcation is indeed not a necessary condition for a power-law behavior.

C. Power-law distribution

As the uniform threshold distribution may be a little bit artificial, one should consider some other threshold distributions. Among them, the power-law distribution is particularly instructive as the system exhibits more complex behaviors than the uniform distribution case. It is also important in view of the geophysical systems as the heterogeneities in solid earth systems are often fractal.

The threshold distribution $p(f)$ is proportional to $f^{-\alpha}$ ($\alpha > 0$) within the range of $[f_{\min}, f_{\max}]$ and vanishes otherwise. For $\alpha \neq 1$, the distribution reads

$$p(f) = \frac{1 - \alpha}{f_{\max}^{1-\alpha} - f_{\min}^{1-\alpha}} f^{-\alpha}. \tag{32}$$

This leads to

$$\Phi(f) = \begin{cases} \frac{f_{\min}^{1-\alpha} - f_{\max}^{1-\alpha}}{f^{1-\alpha} - f_{\max}^{1-\alpha}} f_0, & (f \geqslant f_{\min}) \\ f_0 & (f < f_{\min}) \end{cases}. \tag{33}$$

Then the time evolution equation is given by

$$\dot{f} = \frac{f_{\min}^{1-\alpha} - f_{\max}^{1-\alpha}}{f^{1-\alpha} - f_{\max}^{1-\alpha}} f_0 - f, \tag{34}$$

and therefore the fixed points are the solution of

$$f\left(f^{1-\alpha} - f_{\max}^{1-\alpha}\right) = f_0\left(f_{\min}^{1-\alpha} - f_{\max}^{1-\alpha}\right), \tag{35}$$

where $f_{\min} \leqslant f < f_{\max}$. Noting that the right-hand side of the above equation is a constant, the nature of the fixed points depends on the behavior of the left-hand side, which largely depends on the exponent α. As explained below, the saddle-node bifurcation occurs only for $\alpha < 2$, and therefore the power-law behavior is not expected for $\alpha \geqslant 2$. Nevertheless, the inverse Omori law is observed at $\alpha = 2$. This illustrates that the bifurcation is not a necessary condition of the power-law behaviors.

(1) For $\alpha > 2$, the left-hand side of Eq. (35) is a monotonically decreasing function from the infinity to the negative infinity as f varies from zero to the infinity. Therefore, in view of Eq. (34), there must be one unstable fixed point. In this case, the system fails quickly starting from f_0 that is larger than a critical value, f_0^*. This is given by inserting $f = f_0 = f_0^*$ in Eq. (35). Therefore, the power-law behavior is not observed for $\alpha > 2$.

(2) For $\alpha < 2$, the left-hand side of Eq. (35) is a concave function of f for $0 < \alpha < 1$, or convex for $1 < \alpha < 2$. Therefore, there must be two fixed points at sufficiently small f_0, and they should merge at a critical value of f_0. Namely, saddle-node bifurcation occurs. This bifurcation point is determined by combining Eq. (35) and

$$\Phi'(f) = (\alpha - 1)\frac{f_{\min}^{1-\alpha} - f_{\max}^{1-\alpha}}{\left(f^{1-\alpha} - f_{\max}^{1-\alpha}\right)^2} f_0 f^{-\alpha} = 1. \tag{36}$$

Equations (35) and (36) lead to

$$f\left(f^{1-\alpha} - f_{\max}^{1-\alpha}\right)\left[2 - \alpha - \left(\frac{f}{f_{\max}}\right)^{\alpha-1}\right] = 0, \tag{37}$$

which gives

$$f = (2-\alpha)^{1/(\alpha-1)} f_{\max}. \tag{38}$$

The critical initial condition is given by inserting the above equation to Eq. (35):

$$f_0 = \frac{(\alpha-1)(2-\alpha)^{(2-\alpha)/(\alpha-1)}}{f_{\min}^{1-\alpha} - f_{\max}^{1-\alpha}} f_{\max}^{2-\alpha}. \tag{39}$$

We can thus expect the power-law behaviors of $f(t)$ for $0 < \alpha < 1$ and $1 < \alpha < 2$. This is confirmed by numerical simulation as shown in the next section.

(3) For $\alpha = 2$, the left-hand side of Eq. (35) is a monotonically decreasing function, and therefore there exists one unstable fixed point as in the case of $\alpha > 2$. Nevertheless, one may observe power-law behavior. The time evolution equation reads

$$\dot{f} = \frac{f_{\min}^{-1} - f_{\max}^{-1}}{f^{-1} - f_{\max}^{-1}} f_0 - f. \tag{40}$$

If we choose $f_0 = (f_{\min}^{-1} - f_{\max}^{-1})^{-1}$, the above equation reduces to

$$\dot{f} = \frac{f^2/f_{\max}}{1 - f/f_{\max}}, \tag{41}$$

which have a solution of $f \propto (t_f - t)^{-1}$ unless $f/f_{\max} \simeq 1$. In this case, however, the power-law behavior is observed even if the bifurcation does not occur.

(4) For $\alpha = 1$, the distribution reads

$$p(f) = \frac{1}{f \log\left(\frac{f_{\max}}{f_{\min}}\right)}. \tag{42}$$

By computing $\Phi(f)$, the fixed points are given by the following equation:

$$f \log\left(\frac{f}{f_{\max}}\right) = f_0 \log\left(\frac{f_{\min}}{f_{\max}}\right). \tag{43}$$

We can also show that the saddle-node bifurcation occurs at $f_0 = f_{\max}/e \log(f_{\max}/f_{\min})$ and $f = e^{-1} f_{\max}$, and therefore we can expect power-law behaviors.

IV. NUMERICAL RESULTS: GLOBAL LOAD SHARING MODEL

In the following, numerical results are shown for both the GLS and the LLS models. In each case, the system comprises 10^5 fibers and the results are averaged over 10^4 configurations. The main aim for the numerical study is to confirm the analytical results given in the previous section as well as to understand the time evolution of the system with more general threshold distributions. In the case of the GLS model, we have used three different threshold distributions: uniform, Weibull, and power laws. The numerical results are compared with the analytical ones. In case of the LLS model, the numerical results shown here are restricted to the uniform threshold distribution only.

For both the systems (GLS and LLS), we show the strain rate as a function of time in the system under a constant load, which is slightly above the critical value. Using the number of unbroken fibers after the tth redistribution (at time t), which is denoted by L_t, the strain $\epsilon(t)$ is represented as F/L_t with the force F applied to the system. This is indeed identical to the force per fiber f in the GLS model. However, in the LLS model, this strain may be interpreted as the average value (averaged over all surviving fibers), as the force per fiber is inhomogeneous. In the same manner, the strain rate is given as the time derivative of the average strain: $\dot{\epsilon}_t = F/L_{t+1} - F/L_t$. Again, this is identical to $\dot{f}$ in the GLS model, whereas it is the averaged value in the LLS model.

A. Uniform threshold distribution: Comparison of analytical and numerical results

Here the threshold of each fiber is chosen from a uniform distribution defined on the interval of $[0.5 - \delta, 0.5 + \delta]$.

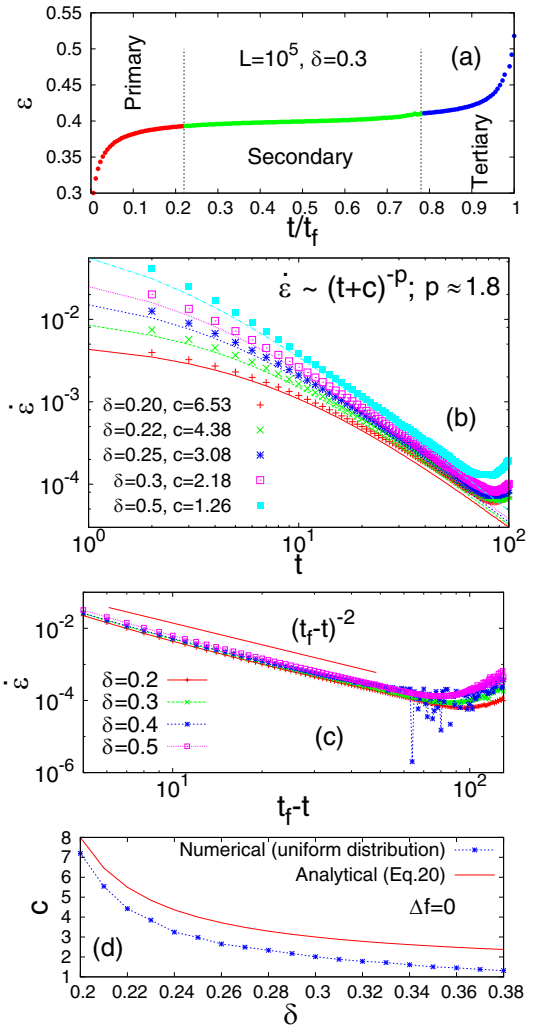

FIG. 2. (a) Behavior of strain, showing the primary, secondary, and tertiary stages in the time evolution normalized by failure time t_f. [(b), (c)] Variation of the strain rate with time respectively in the primary and tertiary stages, along with the comparison with the analytical findings (lines with no points). (d) Variation of c value with δ, the strength of disorder, in the primary stage.

Figure 2(a) shows the creeplike behavior observed under such critically stressed condition. The behavior shows all three stages: primary (red), secondary (green), and tertiary (blue). The strain rate at primary and tertiary stage is observed closely and shown in Figs. 2(b) and 2(c) respectively.

The time evolution of strain rate in the primary stage [Fig. 2(b)] follows the Omori-Utsu law and matches satisfactorily with the analytical expression [solid lines drawn according to Eq. (19)]. Also in the tertiary stage, the numerical results match with the inverse Omori law given by Eq. (22). We will discuss this in details later in this paper. Also Fig. 2(d) compares the analytical [see Eq. (20)] and numerical c values at different degrees of disorder, under the condition $f = f_c$. A probable reason for the discrepancies between analytical and numerical results is the assumption made in Eq. (18).

B. Weibull distribution

If the constituent fibers themselves are sufficiently macroscopic objects, the strength of a single fiber may obey extreme statistics. Earlier studies indicate that materials show scatter in their strength, the distribution of which can be represented by a long-tailed Weibull distribution [36,37]. In light of that, one can consider the Weibull distribution for the fiber strength.

$$\int_f^\infty p(y)dy = \exp\left[-\left(\frac{f}{\widetilde{f}}\right)^\beta\right], \tag{44}$$

where $\beta > 0$ and $\widetilde{f}$ is a constant. This leads to the time evolution equation,

$$\tau\dot{x} = x_0 \exp(x^\beta) - x, \tag{45}$$

where $x = f/\widetilde{f}$.

Whereas the uniform distribution case is controlled by the only one dimensionless parameter, the Weibull distribution case involves two dimensionless parameters, β and x_0. Note that very large or very small β values correspond to less heterogeneity and the intermediate values of β may represent disordered systems. However, the parameter β does not affect the qualitative behavior of the system as shown below.

1. Saddle-node bifurcation

First, we show saddle-node bifurcation also occurs for the Weibull distribution case irrespective of the value of β. The fixed points of Eq. (45) must satisfy

$$x_0 \exp(x^\beta) = x. \tag{46}$$

Since $x > 0$, it is more convenient to take the logarithm:

$$x^\beta - \log x = -\log x_0. \tag{47}$$

As the left-hand side is a simple concave function of x for positive β, the above equation must have two solutions at sufficiently small x_0. One can show that the smaller solution is the stable fixed point, whereas the larger one is unstable. At a critical value of $x_0 = (e\beta)^{-1/\beta}$, these two fixed points merge and disappear. This is the saddle-node bifurcation as in the case of the uniform threshold distribution. For $x_0 > (e\beta)^{-1/\beta}$, there is no fixed point and the force per fiber increases rapidly with time. Therefore, we can expect the power-law behaviors with the exponent 2 as discussed in the previous section.

2. Dependence on disorder β

To check the response of the model to the disorder introduced, we have studied the variation of strain rate ($\dot{\epsilon}$) with time at different disorder values while the applied stress is kept constant at the critical value.

Figure 3 shows the strain rate as a function of time with a continuous change in β (and hence change in disorder). Here also we observe the Omori and inverse Omori laws in the primary and tertiary stages, respectively:

(1) primary stage: $\dot{\epsilon} = \dfrac{k}{(t+c)^p}$, $p \approx 1.8$,

(2) tertiary stage: $\dot{\epsilon} = \dfrac{k'}{(t_f - t)^{p'}}$, $p' \approx 2.0$,

where t_f is the time of breakdown of the system.

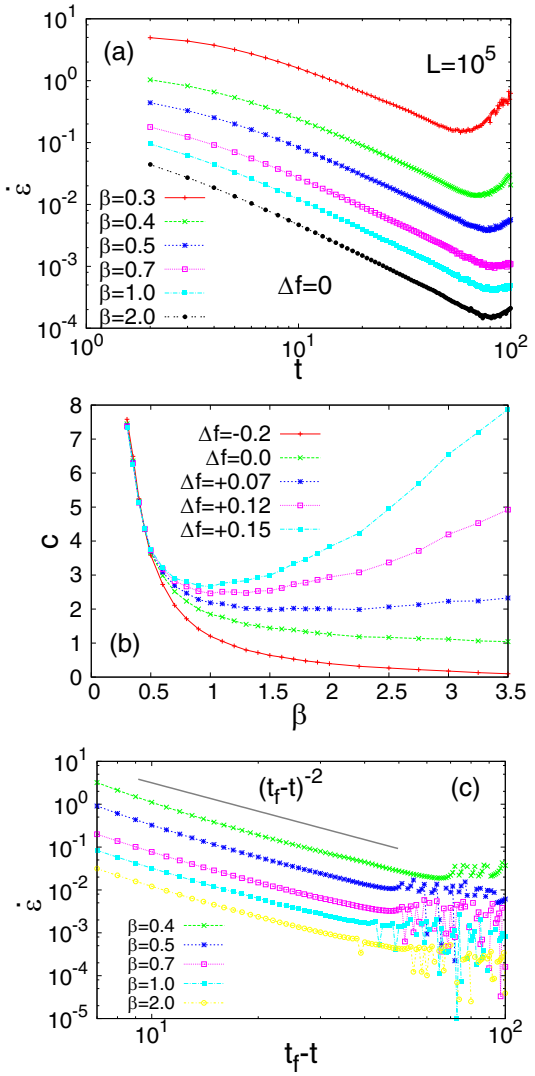

FIG. 3. Time evolution of the model with Weibull threshold distribution. (a) Omori-like behavior in the primary stage with a continuous variation of disorder. (b) Variation of c value with disorder at different loading conditions. (c) Inverse-Omori-like behavior close to the failure point.

Both exponents p and p' show satisfactory match with the analytical results. In the primary stage, the value of c changes with a continuous variation of β. The applied stress is kept constant here at the critical value. Strain rate produced in the model at critical stress and corresponding to different β values [see Fig. 3(a)] in the primary stage are fitted with the Omori law for different c values. The variation of c value with β is shown in Fig. 3(b) at different loading condition. Δf shows the deviation in applied stress from the critical value f_c. $\Delta f = 0$ corresponds to the critically loading condition. A positive Δf tells us that the model is overloaded, while a negative value of Δf leads to situation where the applied load is less than the critical one. c attains a higher value at both low- and high-β values and hence at low-disorder limit. This nonmonotonic behavior is very prominent where the system is more overloaded ($\Delta f > 0$). For $\Delta f \approx 0$ or $\Delta f < 0$, we have to go to relatively higher value of β to observe this increment

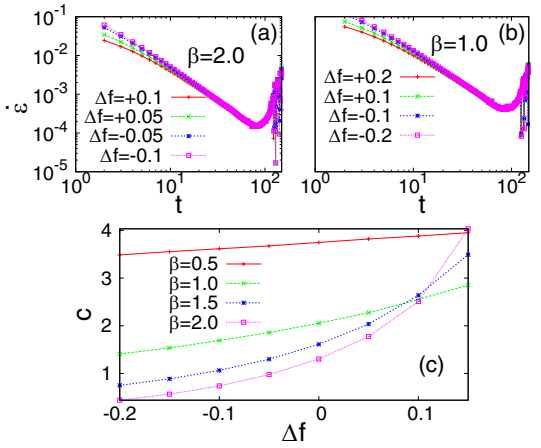

FIG. 4. Omori-like behavior at different loading conditions. [(a), (b)] $\dot{\epsilon}$ vs t for two different disorder values $\beta = 2.0$ and $\beta = 1.0$. (c) Variation of c value with Δf for $0.5 < \beta < 2.0$.

in c value. Finally, Fig. 3(c) shows the strain rate, close to the failure point. When t approaches t_f, $\dot{\epsilon}$ increases in a scalefree manner with an exponent -2, independent of the disorder introduced in the model. Also, as discussed before, we have a zero c value here.

3. Dependence on the applied stress

Next we have investigated the effect of applied stress more closely focusing on the primary stage only.

Figures 4(a) and 4(b) show the Omori-like behavior under different loading conditions. At high-β value, the system responses quite well with varying applied stress. On the other hand, at low-β value, c changes very slowly with Δf. These different responses can be expressed through a continuous variation of c value with Δf. Figure 4(c) shows the c value vs Δf variation at different β (hence at different disorder values). As previously discussed, at low β, c starts with a relatively higher value and gradually increases with Δf. For higher β value, c attains a lower value initially but increases more quickly with Δf. Hence, the rate of change of such c value is relatively higher for high disorder values.

4. Variation of c value on Δf-δ plane

Finally we have reached a point where we can explain the behavior of the c value with respect to the parameters β and Δf. In Figs. 5(a) and 5(b), we have shown the c value in the primary stage as function of both disorder and applied stress in case of the uniform and the Weibull distributions.

The value of c is higher at less disorder (low δ for uniform distribution and very low or very high β for Weibull distribution) and gradually deceases when we go to higher disorder. At any particular δ or β, the c value increases with increasing Δf.

C. Power-law threshold distribution

Next, we have carried out the numerical simulation where the thresholds are chosen randomly from a power-law distribution with a variable exponent. Following the analytical results, we introduce some cutoff values for the distribution depending on

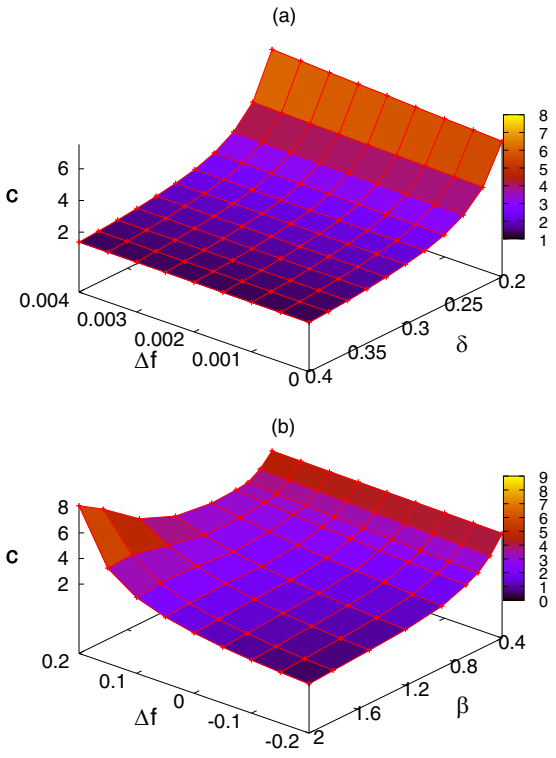

FIG. 5. Variation of c value when both Δf and β are continuously varying parameters. Results are shown for (a) uniform and (b) Weibull distributions.

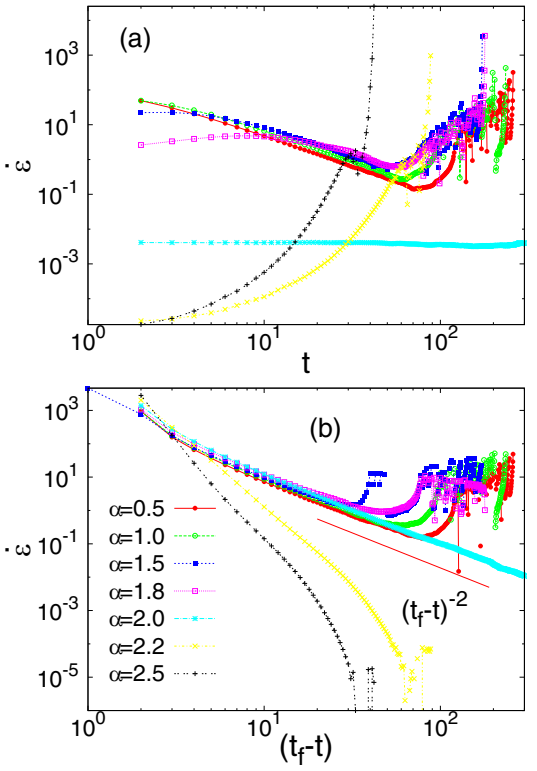

FIG. 6. Strain rate vs time in the (a) primary and (b) tertiary stages of the creep process. The threshold distribution considered here is $p(f) = f^{-\alpha}$ within the window $[1, 10^3]$.

the value of α. Irrespective of the value of α, we must choose a sufficiently large width that remains constant throughout the numerical simulation. Here it is chosen to be $[1, 10^3]$, where the exponent α varies between 0.5 and 2.5. This variation in the exponent essentially covers all the three situations discussed in the analytical study (see Sec. III C).

Figure 6 illustrates the behaviors of strain rate in the primary and the tertiary stages, respectively, where the qualitative difference is apparent for different values of the exponent α:

(i) For $\alpha < 2$, we obtain a power-law decrease of strain rate $\dot{\epsilon}$ in the primary stage. At the same time, in the tertiary stage $\dot{\epsilon}$ increases, obeying the inverse Omori law until it reaches global failure. The p values at primary and tertiary stages are respectively 1.8 and 2.0.

(ii) For $\alpha > 2$, the model shows brittle response. In this limit, $\dot{\epsilon}$ increases exponentially in the primary stage and reaches to global failure much more rapidly and does not exhibit the inverse Omori law in the tertiary stage.

(iii) At $\alpha = 2$, the power-law behavior is observed only in the form of inverse Omori law while the strain rate is almost constant in the primary regime. All these behaviors are consistent with the analytical results.

V. NUMERICAL RESULTS: LOCAL LOAD-SHARING MODEL

In this section, we have studied a one-dimensional fiber bundle model with local load-sharing scheme. To model stress concentration at the crack tip, we assume that the close neighborhood of broken fibers is loaded much more than the rest. Namely, the load supported by a broken fiber is redistributed over a finite distance, known as the stress release range R. A recent study has already shown that there exits the critical range value R_c, above which the model shifts to the mean-field limit. The critical value depends on the system size L as $R_c \sim L^{2/3}$ [38] (where threshold strength values are chosen from a uniform distribution [0,1]). In this paper, instead of R, we have used $\rho = R/R_c$ as the parameter, and thus $\rho \geqslant 1$ corresponds to the mean-field limit of the model.

Throughout this section, the uniform threshold distribution is adopted and therefore we investigate the effects of disorder by changing δ, as well as the effects of the interaction range by changing ρ. Again, the external load remains to be slightly above the critical value.

A. Memory effect

In a conventional one-dimensional LLS fiber bundle model with $R = 1$, the load supported by a broken fiber is equally redistributed between its two nearest intact fibers [see Fig. 7(a)]. In this algorithm, the stress accumulated near the two crack tips of a certain crack can be unequal [39,40]. Namely, the local stress at one crack tip can be larger than the other one. For example, Fig. 7(a) shows that the local stress on the crack tips becomes asymmetric after two consecutive rupture events. The details of this left-right asymmetry depends on the history of failure process.

A different algorithm that eliminates this effect has been known in the literature [41]. According to this algorithm, an intact fiber with n_l broken fibers on the left side and n_r broken

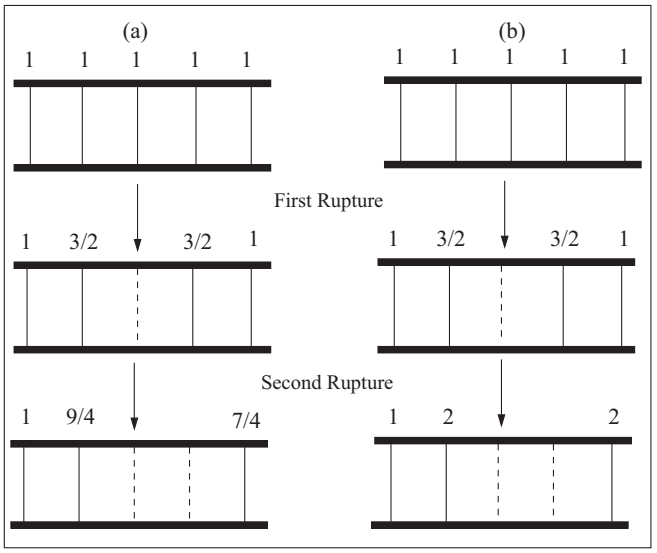

FIG. 7. Schematic diagram of fiber bundle model, showing the effect of memory during the rupture events. The dashed line shows a ruptured fiber. (a) In the case of the conventional model, the local stresses on the crack tips are uneven. (b) After memory is removed from the model, both the tips carries the same stress.

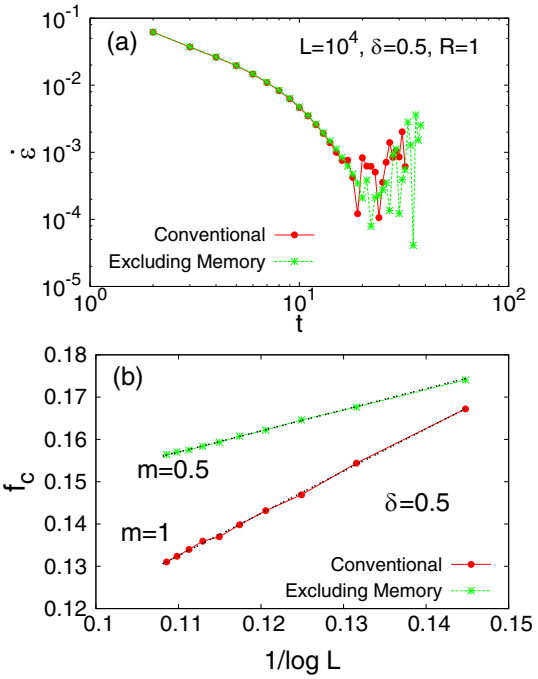

FIG. 8. (a) Time evolution of strain rates in the conventional algorithm and the memory-free algorithm. Each curve is obtained at the critical stress, which depends on the algorithm. (b) System-size effect on the critical stress (f_c) for each algorithm. In both cases, it is described by $f_c = a - m/\log L$, where log denotes the natural logarithm. For the conventional algorithm, $m = 1.0$ and $a = 0$. The coefficient m decreases to 0.5 for the memoryless algorithm, where the critical stress is higher. The constant a also shifts to a nonzero value ($\approx$0.1).

fibers on the right side will carry a stress of $[1 + (n_l + n_r)/2]f$, where f is the stress per fiber applied externally. Note that n_r and n_l are the cumulative number of broken fibers from $t = 0$. Figure 7(b) shows the rupture events when the external stress per fiber is unity ($f = 1$). After one fiber breaks (denoted by the dotted line) in the first rupture event, the stress on the fiber on its left will be 3/2 as in this case $n_r = 1$ (the broken fiber itself) and $n_l = 0$. At the same time, the stress on the fiber on its right will also be 3/2 but here $n_l = 1$ (the broken fiber itself) and $n_r = 0$. After the second rupture event that yields two consecutive broken fibers, the fiber on the left side of the patch will have the stress of 2. In this case, $n_r = 2$ (two broken fibers) and $n_l = 0$. The fiber on the right side of the patch will also have the stress of 2. Here, $n_r = 0$ and $n_l = 2$ (two broken fibers). Following this algorithm, we get equal local stress of 2 on the crack tips and the failure events are no longer history dependent.

Let us assume that L_t^m is the number of unbroken bonds at time t in the conventional algorithm and L_t^{wm} is the number for the memoryless algorithm. As the symmetric stress distribution results in more stable dynamics, we can expect $L_t^{wm} > L_t^m$ if the external load F is the same. As the strain is given by $\epsilon = F/L_t$, the system with the memoryless algorithm will be less strained at a certain time t. Therefore, the strain ϵ and the strain rate $\dot{\epsilon}$ may generally depend on the time-evolution algorithm under the same external load.

B. Critical stress

Importantly, the time evolution of strain rate is rather insensitive to a specific algorithm as long as the critical load is applied to the system. The comparison of the above two algorithms is shown in Fig. 8(a) with $L = 10^4$, $\delta = 0.5$, and $R = 1$. Note that the two curves are obtained at different external loads, as each algorithm has different critical stress.

Since the model is stabilized when the memory is removed, we need to increase the external load in order to break the whole bundle. Namely, the critical stress is affected by the memory. This is shown in Fig. 8(b) for $R = 1$ and $\delta = 0.5$. The numerical result indicates that $f_c \sim a - m/\log L$, where L denotes the system size. Such a behavior was observed in the literature of fiber bundle model, both analytically [34] and numerically [20]. The only difference is the slope m of above equation shifts from 1.0 to 0.5 as the memory is removed. Additionally, a vanishes for the conventional model while it takes a nonzero value ($a \approx 0.1$) when memory is removed. This means that a higher critical stress is required for the memoryless algorithm at any system size L. Namely, we obtain $f_c^{wm} > f_c^m$, where f_c^m and f_c^{wm} are the critical stress values with and without memory, respectively. However, the strain $\epsilon = f_c/(L_t/L)$ may be less sensitive to the specific choice of algorithm as both f_c and L_t increase (or decrease) in the memoryless (or conventional) algorithm. This might be the possible reason behind the algorithm-independent results for strain rate in our present work.

C. Time evolution of strain rate

Below we have studied the time evolution of $\dot{\epsilon}$ at the critical stress f_c with local load-sharing scheme for different disorder

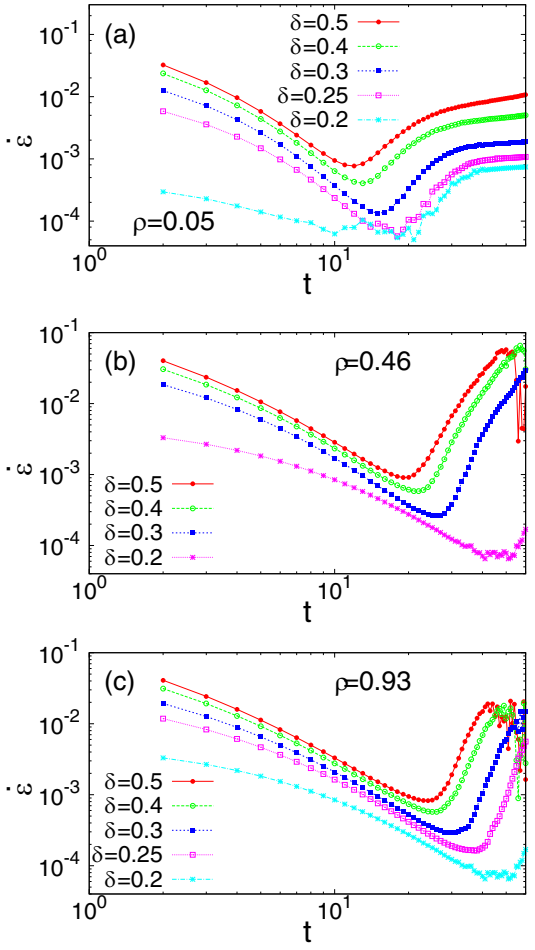

FIG. 9. Variation of strain rate with time (in the primary stage) for disorder δ, ranging in between 0.2 and 0.5, while a critical stress is applied on it. The study is repeated for $\rho = 0.93$, 0.46, and 0.05.

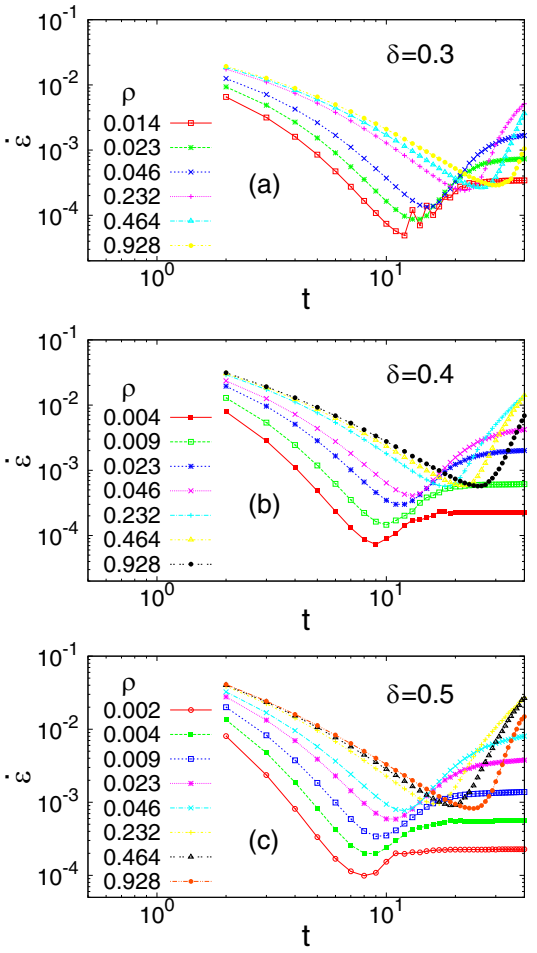

FIG. 10. Plot for $\dot{\epsilon}$ vs t in the primary stage at three different disorder values ($\delta = 0.3$, 0.4, and 0.5). The stress is kept constant at the critical value while ρ is continuously varied.

strength δ and stress-release range ρ. We observe the strain rate to independent of memory at $R = 1$. As R increases, the model gradually approaches the mean-field limit. Also the effect of memory vanishes gradually at the same time. As $\dot{\epsilon}$ is independent of memory for $R = 1$, we can expect that the results will hardly be affected by the memory for higher R values. Since the strain rate is not affected by memory, it does not matter whether the memory for the following results are removed or not.

1. Role of disorder

Figure 9 shows the behavior of strain rate in the primary stage with different values of local stress concentration parameter ρ: 0.93, 0.46, and 0.05. In the case of $\rho = 0.05$, the stress is redistributed up to a small range, whereas $\rho = 0.93$ is close to the mean-field limit. As a result, it is expected to obtain the Omori-Utsu law in the primary stage when the ρ is close to 1 [see Fig. 9(c)]. Interestingly, we observe this behavior to be sustained even for lower ρ, namely more stress localization. The c value also changes with disorder in this limit. The extra feature that we get with stress localization is a varying exponent p in the Omori-Utsu law.

2. Role of stress-release range

Here we have studied the model at a constant disorder but with varying stress-release range. By changing a variable ρ, the model shifts from the mean-field limit to another limit where stress redistribution is extremely localized.

Figure 10 shows the time evolution of the strain rate with several values of ρ. The study is repeated for three different disorder values. The slope in the Omori-like behavior clearly shows an increment while ρ is decreased. Also at very low ρ, the exponent p changes with disorder. This variation of p with disorder was absent in the mean-field limit.

3. Variation of c value and exponent p

To understand the effect of such stress localization, we have studied the c value and the exponent p with a continuous variation of stress-release range ρ between 0 and 1.5 (see Fig. 11). As we have already mentioned, for $\rho \geqslant 1$ the model enters its mean-field limit.

For smaller interaction range ($\rho < 1$), both p and c take large values. As ρ is increased, these two quantities decrease gradually. Throughout the stage $0 < \rho \leqslant 1.5$, the c value remains a function of disorder δ and increases as we go to

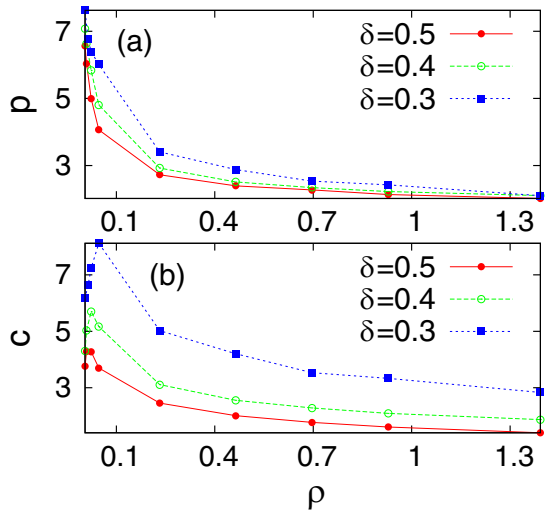

FIG. 11. Variation of the c value and and the exponent p with increasing stress localization. The model approaches the mean-field limit toward $\rho = 1$, and p approaches its mean-field value 1.8 gradually with increasing ρ.

lower δ values. So, c can be expressed as follows: $c = \Phi(\rho,\delta)$ for $0 < \rho \leqslant 1.5$, where Φ is an decreasing function of both stress-release range ρ and disorder δ. On the other hand, the exponent of p is function of both disorder δ and stress localization ρ for $\rho < 1.0$. For $\rho > 1.0$, p takes a value 1.8 independent of δ and ρ, which is the mean-field exponent for Omori law we obtained previously.

With local stress concentration (the LLS scheme), the strain rate increases rapidly in the tertiary region until all the fibers break. Though, unlike the mean-field limit, the strain rate does not show the inverse Omori behavior here.

The results in the mean-field limit are already shown for three different distributions: uniform, Weibull, and power law. An universal behavior is observed in the time evolution of strain rate (or force per fiber) for all these three distributions. With local stress concentration, we have shown the results with uniform distribution. The universality of these results are also checked with a Weibull distribution with shape parameter β and a power-law distribution with exponent -1 ranging from $10^{-\eta}$ to 10^{η}. The parameters η and β control the disorder here.

VI. DISCUSSION

Here we discuss the relevance of the Omori-Utsu and the inverse Omori laws in a more general context. Although our results are presented in terms of the strain rate, they should apply to more general cases if there is a relation between the rate of microfracture events and the strain rate, such as $n(t) \propto \dot{\epsilon}(t)^q$, where $n(t)$ is the rate of microfracture events and q is a positive exponent. As the rupture of a single fiber may correspond to a single microfracture event in the present system, $n(t) \propto \dot{\epsilon}(t)L^2(t)$, where $L(t)$ is the number of remaining fibers at time t.

Noting that aftershocks are caused by the abrupt stress change caused by a main shock, the algorithm adopted here, in which a finite stress is applied to the system at $t = 0$, may model such a stress change caused by a main shock. In this sense, the Omori-Utsu law obtained in the present model mimics the dynamics after a main shock for earthquakes to some extent. We obtain the exponent $p \simeq 2$ in the mean-field model irrespective of the other details such as the threshold distribution, whereas p ranges from 0.6 to 0.8 in the creep test and from 0.7 to 1.6 for earthquakes. The difference is significant but the quantitative agreement is not necessarily here because of the simplicity of the mean-field model. In contrast, the difference is even larger for the LLS model. Noting that the LLS model is generally more unstable than the GLS model, we may obtain smaller exponent for more stable systems. For instance, introducing a probabilistic rule for the elementary fracture process might lead to smaller exponent because it can inhibit the cascade-like instability of fracture caused by the load redistribution to slow down the relaxation.

The c value is a characteristic time for the power-law relaxation that results from the abrupt stress loading and therefore it is regarded as a relaxation time for stress. The elementary stress relaxation time in our model is τ, which makes a single time step. It is indeed the only intrinsic time constant in our model and therefore the c value should be scaled with τ from dimensional analysis. The c value is thus mostly dominated by the nature of τ. For instance, if the stress relaxation time depends on the total load F, the analysis given in this study still applies and yields the load-dependent c value.

In the GLS model, the analytical expression for the c value is obtained for a class of threshold distributions. Apart from the trivial dependence on τ, the c value depends on three parameters: a, f_c, and f_0. Among them, a and f_c are determined mostly by the threshold distribution via Eqs. (24) and (26) but they also depend on f_0 because $\Phi(f)$ is proportional to f_0. Therefore, a should be proportional to f_0. Noting that f_0 is proportional to the total load F as $f_0 = F/L_0$, Eq. (31) implies the load dependence of the c value. Although the c value is found to increase with the load in this study, in view of Eq. (31), it can be a decreasing function of the external load if $f_c > 2f_0$. This actually means $f_c > 2f_0^*$ and therefore it depends on the threshold distribution. This condition is not satisfied for the distribution functions investigated here and hence the c value exhibits only positive dependence on the external load.

VII. CONCLUSIONS

We have studied the time evolution of fiber bundle model under a constant external load being slightly above the critical value with some variations in the load redistribution process: the global load-sharing and the local load-sharing models. The strain rate in the primary and the tertiary stages follows the Omori-Utsu and the inverse Omori laws respectively. In the local load-sharing model, both the exponent p and the c value are decreasing functions of disorder and the interaction range. Above a certain stress-release range ($\rho > 1$), the local load-sharing model exhibits essentially the same behavior as that of the mean-field limit; namely, the exponent for the Omori-Utsu law attains a constant value ($\approx$1.8) and c is still a decreasing function of disorder. Despite the simplicity of the model and the absence of any thermal activation process, the system exhibits creeplike behaviors with all the three stages: primary, secondary, and tertiary. This in turn implies that the probabilistic rule is not essential for a power-law behavior in creep deformation.

In this study, the fiber interaction is incorporated only as the aftermath of fiber rupture redistributing the load to all the rest fibers or the neighboring fibers in the bundle. However, one can consider other specific types of interactions. For instance, the amount of force redistribution may decay in space as a power law [42]. Yet another interesting model is the fibers on a complex network [43], which may model some social or economic systems. These are some of the interesting directions for which the present study is to be generalized.

ACKNOWLEDGMENTS

This study was supported by the MEXT under "Exploratory Challenge on Post-K computer" (Frontiers of Basic Science: Challenging the Limits) and the "Earthquake and Volcano Hazards Observation and Research Program." Additional support in the form of JSPS KAKENHI Grants No. JP16H06478 and No. 15H03698, and by the Earthquake Research Institute cooperative research program is gratefully acknowledged.

[1] E. N. Da C. Andrade, Proc. R. Soc. London, Ser. A **84**, 1 (1910).
[2] H. Nechad, A. Helmstetter, R. El Guerjouma, and D. Sornette, Phys. Rev. Lett. **94**, 045501 (2005).
[3] H. Nechad, A. Helmstetter, R. El Guerjouma, and D. Sornette, J. Mech. Phys. Solids **53**, 1099 (2005).
[4] M. Leocmach, C. Perge, T. Divoux, and S. Manneville, Phys. Rev. Lett. **113**, 038303 (2014).
[5] M.-C. Miguel, A. Vespignani, M. Zaiser, and S. Zapperi, Phys. Rev. Lett. **89**, 165501 (2002).
[6] T. Hirata, J. Geophys. Res. **92**, 6215 (1987).
[7] A. Schubnel, B. D. Thompson, J. Fortin, Y. Guéguen, and R. P. Young, Geophys. Res. Lett. **34**, L19307 (2007).
[8] F. Omori, J. Coll. Sci., Imp. Univ. Tokyo **7**, 111 (1894).
[9] T. Utsu, J. Fac. Sci. Hokkaido Univ. Ser. VII (Geophys.) **3**, 129 (1969).
[10] T. Utsu, Y. Ogata, and R. S. Matsuura, J. Phys. Earth **43**, 1 (1995).
[11] R. Shcherbakov, D. L. Turcotte, and J. B. Rundle, Geophys. Res. Lett. **31** (2004).
[12] M. Bouchon, V. Durand, D. Marsan, H. Karabulut, and J. Schmittbuhl, Nat. Geosci. **6**, 299 (2013).
[13] C. Narteau, S. Byrdina, P. Shebalin, and D. Schorlemmer, Nature (London) **462**, 642 (2009).
[14] P. Shebalin and C. Narteau, Nat. Commun. **8**, 1317 (2017).
[15] F. T. Pierce, J. Text. Ind. **17**, 355 (1926).
[16] H. E. Daniels, Proc. R. Soc. London, Ser. A **183**, 405 (1945).
[17] S. Pradhan, A. Hansen, and B. K. Chakrabarti, Rev. Mod. Phys. **82**, 499 (2010).
[18] A. Hansen, P. C. Hemmer, and S. Pradhan, *The Fiber Bundle Model: Modeling Failure in Materials* (Wiley VCH, Berlin, 2015).
[19] S. Ciliberto, A. Guarino, and R. Scorretti, Phys. D (Amsterdam, Neth.) **158**, 83 (2001).
[20] S. Pradhan and B. K. Chakrabarti, Int. J. Mod. Phys. B **17**, 5565 (2003).
[21] R. Shcherbakov and D. L. Turcotte, Theor. Appl. Fract. Mech. **39**, 245 (2003).
[22] Y. Ben-Zion and V. A. Lyakhovsky, Geophys. J. Int. **165**, 197 (2006).
[23] A. Saichev and D. Sornette, Phys. Rev. E **71**, 016608 (2005).
[24] Z. Danku and F. Kun, Sci. Rep. **3**, 2688 (2013).
[25] S. Pradhan and B. K. Chakrabarti, Phys. Rev. E **65**, 016113 (2001).
[26] S. Pradhan and P. C. Hemmer, Phys. Rev. E **75**, 056112 (2007).
[27] S. L. Phoenix, Adv. Appl. Probab. **11**, 153 (1979).
[28] R. L. Smith and S. L. Phoenix, J. Appl. Mech. **48**, 75 (1981).
[29] W. I. Newman and S. L. Phoenix, Phys. Rev. E **63**, 021507 (2001).
[30] D. G. Harlow and S. L. Phoenix, J. Compos. Mater. **12**, 314 (1978).
[31] D. G. Harlow and S. L. Phoenix, Adv. Appl. Probab. **14**, 68 (1982).
[32] R. L. Smith, Proc. R. Soc. London, Ser. A **382**, 179 (1982).
[33] S. Roy and P. Ray, Europhys. Lett. **112**, 26004 (2015).
[34] J. B. Gómez, D. Iñiguez, and A. F. Pacheco, Phys. Rev. Lett. **71**, 380 (1993).
[35] S. Roy, Phys. Rev. E **96**, 042142 (2017).
[36] Z. P. Bažant, S. D. Pang, M. Vořechovsky, D. Novák, and R. Pukl, in *Proceedings of the IA-FraMCoS Fracture Mechanics of Concrete Structures*, edited by V. C. Li, K. Y. Leung, K. J. Willam, and S. L. Billington (Aedificatio Publishers, Freiburg, 2004), Vol. 1, p. 189.
[37] A. Carpinteri, Int. J. Solids Struct. **31**, 291 (1994).
[38] S. Biswas, S. Roy, and P. Ray, Phys. Rev. E **91**, 050105(R) (2015).
[39] D. G. Harlow and S. L. Phoenix, J. Compos. Mater. **12**, 195 (1978).
[40] D. G. Harlow and S. L. Phoenix, J. Mech. Phys. Solids **39**, 173 (1991).
[41] M. Kloster, A. Hansen, and P. C. Hemmer, Phys. Rev. E **56**, 2615 (1997).
[42] R. C. Hidalgo, Y. Moreno, F. Kun, and H. J. Herrmann, Phys. Rev. E **65**, 046148 (2002).
[43] D. H. Kim, B. J. Kim, and H. Jeong, Phys. Rev. Lett. **94**, 025501 (2005).